BLOW-DOWN TESTS CONFIRM ACCURATE CRITICAL FLOW VENTURI MEASUREMENTS DURING TRANSIENTS

John D. Wright
NIST Fluid Metrology Group
100 Bureau Drive, Mail Stop 8361
(301) 975-5937 voice, (301) 258-9201 fax, john.wright@nist.gov

Abstract: Critical flow venturis (CFVs) can be used to measure flow under transient pressure, temperature, and flow conditions with k = 2 uncertainties of 0.4 % or less. Blow-down tests transferred 630 g of nitrogen during a 100 s interval from an unregulated cylinder (initially at 10 MPa) through a CFV into a known collection volume. Fast pressure and temperature sensors monitored the inlet to the CFV. The integrated CFV mass flows, $\int \dot{m}\,dt$, averaged 0.38 % smaller than the mass $\Delta\rho V$ of the collected gas. To reduce temperature transients at the CFV, a heat exchanger was added upstream of it. The heat exchanger reduced the percentage difference $100(\int \dot{m}\,dt\,/(\Delta\rho V) - 1)$ to 0.04 %. Accurate measurements of transient flows require careful measurements of the gas temperature near the throat of the CFV and careful attention to thermal effects on the CFV discharge coefficient. We conclude that a properly instrumented critical nozzle can be used as a flow reference to evaluate the performance of other flowmeter types exposed to transient conditions

1. INTRODUCTION

Accurate flow measurements are needed under conditions of transient pressure, temperature, and flow. Three application examples follow.

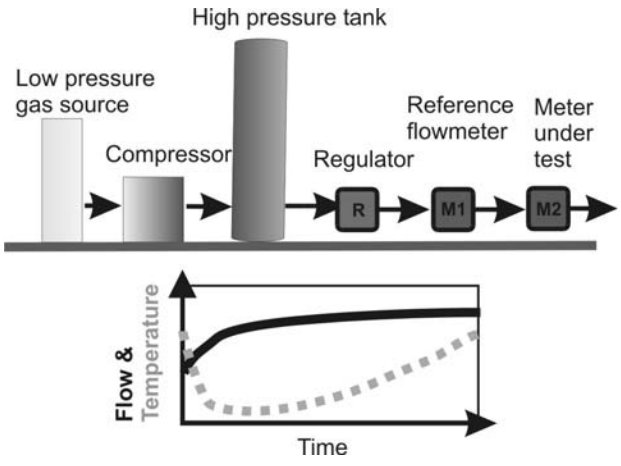

Fig. 1 Schematic of a flow standard using a reference meter and a blow-down tank. Without a heat exchanger, temperature is transient at the reference meter and test section.

Example 1. It is economical to use the arrangement shown in Figure 1 for large gas flow calibrations. A small compressor is used to charge a large pressure vessel over a long period of time. Once the tank is full, a valve on the tank outlet is opened and a pressure regulator is used to achieve approximately stable flow as the tank pressure falls over time. A flowmeter on the discharge serves as a reference to calibrate the meter under test. However, in the absence of a heat exchanger, the temperature of the gas discharged from the regulator will vary over time, introducing errors in the reference flowmeter.

Example 2. Accurate flowmeters are needed for dispensers that sell gaseous fuels for use in vehicles. Figure 2 shows a typical arrangement for a hydrogen gas dispenser. A compressor uses gas from a low pressure source to fill a set of pressure vessels (a cascade tube bank). Valves are sequentially opened to allow gas to flow from each cascade tube to the vehicle tank. As each tube is opened, surges of flow and pressure occur at the flowmeter in the dispenser. Wide temperature changes also occur at the flowmeter and totalized flow errors as large as 10 % have been reported [1]. Another arrangement for refueling gas powered vehicles is direct compression with a reciprocating compressor that generates pulsatile flow at approximately 2 Hz creating a transient flow measurement problem at the billing meter.

Example 3. NIST is constructing a calibration facility to generate accurately measured transient flows. The transient flows will be generated by sequentially opening valves on high pressure cylinders. If the optional regulator and heat

exchanger are not used, the meter under test will be exposed to rapid changes in pressure, temperature and flow mimicking the conditions found in gaseous fuel dispenser applications. The reference flowmeters in this standard will be critical flow venturis (CFVs) [2], previously calibrated by our existing steady-flow *PVTt* standards [3].

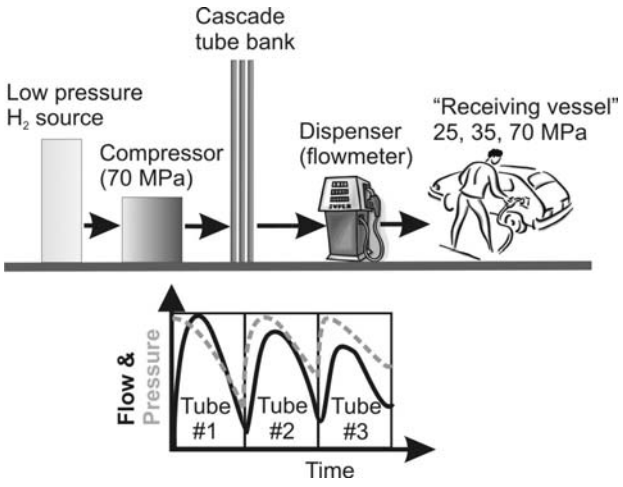

Fig. 2 Schematic of a gaseous fuel dispenser using a cascade tube bank. Flow, pressure, and temperature are all transient at the flowmeter in the dispenser, leading to significant billing errors.

Critical flow venturis can act as accurate flow standards in all of the transient applications described above. To first order, the response time of a CFV equals a characteristic length (*e.g*. throat diameter) divided by the speed of sound; this time is approximately 1 μs in our case.* In practice, transient flow measurements will be limited by the time constants of the pressure and temperature sensors associated with the CFV. Pressure and temperature sensors with time constants < 100 ms are available; exploiting them to determine the flow through a CFV is central to this work.

2. GENERAL DESCRIPTION OF THE EXPERIMENT

To demonstrate the ability of CFVs to accurately measure transient flows, we 1) calibrated a 1 mm diameter CFV under steady temperature, pressure, and flow conditions at pressures up to 13 MPa, 2) instrumented the CFV with fast pressure and temperature sensors and a fast data acquisition system, and 3) conducted blow down tests to check that the integrated CFV flow agrees with the mass of gas collected in a tank (see Figure 3).

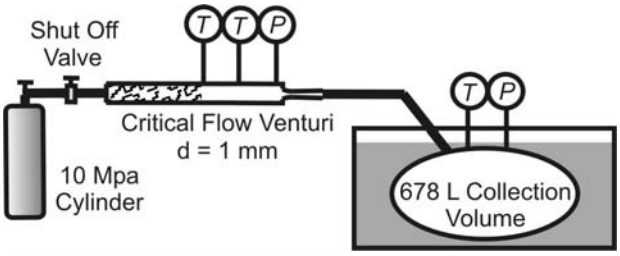

Fig. 3 A schematic of the blow-down test arrangement to study CFV transient performance.

For the blow-down tests, an 8 L cylinder was pressurized with nitrogen to 10 MPa. The pressurized cylinder was the source of gas for the 1 mm CFV. The discharge from the CFV was collected in a 678 L volume. The collection volume and the piping downstream from the cylinder valve were evacuated to < 20 Pa and initial pressure and temperature values were recorded (P_i and T_i). The fast data acquisition system was activated to record the pressure and the temperature at the inlet of the CFV every 50 ms. The shut-off valve was opened for approximately 100 s allowing gas to flow from the pressure vessel into the collection volume. After the pressure in the pressure vessel fell to approximately 900 kPa, the shut-off valve was closed. After the pressure and temperature in the collection volume and piping reached equilibrium, we recorded the final values P_f, and T_f. The mass of gas collected in the tank was calculated via the equation:

$$m_T = V\left(\rho_f - \rho_i\right) \tag{1}$$

where V is the volume of the tank and piping downstream from the CFV (678.726 L), ρ_i is the initial gas density, and ρ_f is the final gas density. The gas density was calculated via a real gas equation of state [4]. The final pressure in the collection volume was approximately 80 kPa, and the mass of nitrogen collected was 630 g. The collection volume was in a temperature controlled

* There are second order effects on CFV flows that are much slower. For example, after a flow change, a long time interval is required to attain a steady temperature distribution in the CFV's body. During this interval, the changing thermal boundary layer in the CFV generates a small, time-dependence of the discharge coefficient.

water bath, ensuring that the measurement of the temperature of the collected gas uncertainty of 12 mK (k = 2) [3].

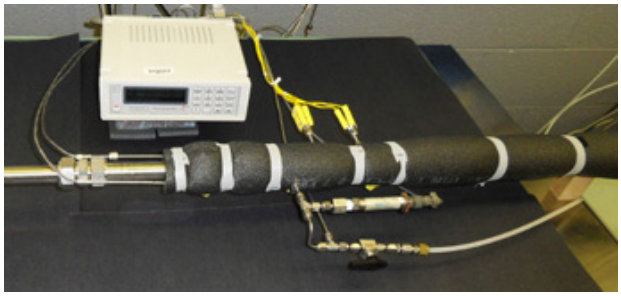

Fig. 4 A photograph of the CFV test section for the blow-down tests.

The mass of gas that flowed through the nozzle into the collection volume was calculated by numerically integrating the CFV flow during the time interval when the shut-off valve was open:

$$m_{\mathrm{CFV}} = \int_{t_i}^{t_f} \dot{m}_{\mathrm{CFV}}\, dt \cong \sum_{k=1}^{n-1} \frac{\dot{m}_k + \dot{m}_{k+1}}{2}\left(t_{k+1} - t_k\right) \qquad (2)$$

where t_i and t_f are initial and final times that span the interval that the shut-off valve was open, t_k are the times at which n discreet CFV flow measurements covering the open valve period were made, and the CFV mass flow $\dot{m}$ is given by:

$$\dot{m}_{\mathrm{CFV}} = \frac{C_{\mathrm{d}} P_0 A C^* \sqrt{\mathscr{M}}}{\sqrt{R T_0}} \qquad (3)$$

where C_{d} is the CFV discharge coefficient, P_0 and T_0 are the stagnation pressure and temperature, A is the throat area, C^* is the real gas critical flow function [4], $\mathscr{M}$ is the molecular mass, and R is the universal gas constant. If the CFV accurately measures flow through transient conditions, then the mass accumulated in the collection volume will equal the integrated CFV flow, *i.e.* $\Delta\rho V = \int \dot{m}\, dt$.

3. EXPERIMENTAL DETAILS

The 1 mm CFV was machined into a 60 ° taper seal high pressure fitting for 25 mm tubing (see Figure 5). The approach tube for the CFV was 70 cm long with inside diameter of 14 mm and the tube exterior was insulated (see Figure 5). The first half of the approach tube was filled with brass wool to promote temperature uniformity across the pipe cross section and to break up the jet resulting from the expansion from 5 mm to 14 mm inside diameters at the approach tube inlet (see Figure 3).

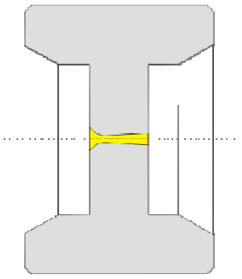

Fig. 5 CFV machined into a high pressure taper seal fitting.

The approach tube had three ports, one for a pressure tap and two for temperature sensors, 23 cm and 16 cm upstream from the CFV inlet. The temperature sensors were exposed Type K thermocouples with wire diameter of 0.05 mm welded onto 0.25 mm supports within a 3 mm insertion tube. Two thermocouple junctions were installed within each 3 mm insertion tube (see Figure 6). The time constant of the thermocouples ranges from 20 ms to 100 ms depending on the flow of gas [5].

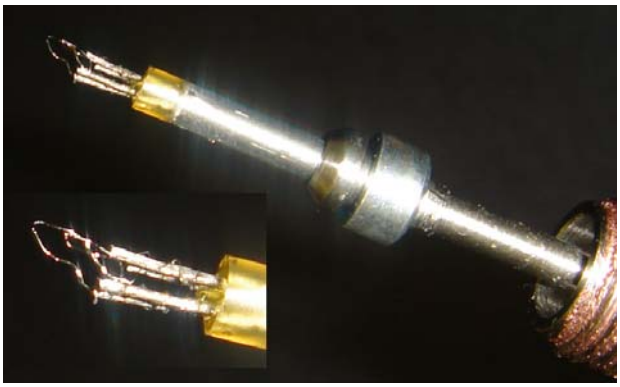

Fig. 6 0.05 mm thermocouple pair.

Even with insulation on the flow tube, heat transfer from the room causes the gas temperature to change as it approaches the CFV. Obtaining accurate CFV gas temperature measurements is a major source of uncertainty in some applications (see Section 6). In these experiments, the two temperature measurements from the streamwise displaced sensors were extrapolated to obtain the temperature at the plane of the CFV inlet and this

temperature was used for all CFV calibrations and flow calculations, *i.e.*,

$$T_1 = tc_3 + \frac{16}{7}(tc_3 - tc_1) \qquad (4)$$

where T_1 is the CFV static temperature, tc_1 and tc_3 are the temperatures measured by thermocouples 1 and 3, and the distances between thermocouples 1 and 3 is 7 cm and the thermocouple 3 is 16 cm from the CFV entrance. T_1 was used to calculate the stagnation temperature T_0 using the corrections found in reference [2].

The manufacturer's specification for the pressure sensor time constant is 3 ms. However, the flow impedance imposed by the pressure tap and tubing between the approach tube and the transducer can slow the time response. Experiments and analytical estimates give a time constant of < 10 ms. During transient tests, data were acquired in 20 s bursts with 50 ms resolution.

Slow pressure sensors were installed in parallel with the fast sensors and they were used under steady state conditions to re-zero the fast sensors before each test. Slow temperature sensors (3 mm sheathed thermistors) were used to measure the temperature at the external surface of the CFV body.

4. STEADY STATE CFV CALIBRATIONS

The CFV was calibrated with > 99.995% purity nitrogen using the NIST 34 L and 678 L *PVTt* flow standards to obtain C_d values at Reynolds numbers between 25×10^3 and 1.4×10^6, covering the range that would occur during the blow-down tests when the pressure dropped from 10 MPa to 200 kPa. The C_d calibrations were performed under approximately steady state conditions using the test arrangement shown in Figure 7. The source of nitrogen was a manifold of 8 cylinders filled to 41 MPa. The regulator was used to maintain pressure at the desired set point. A stirred water bath controlled to match room temperature and 5 m of coiled stainless steel 6.4 mm tubing immersed in the water served as a heat exchanger to return the cold gas exiting the regulator to room temperature. The output from the CFV was connected to the NIST *PVTt* standards which measured mass flow with 0.025 % (k = 2) * uncertainty [6].

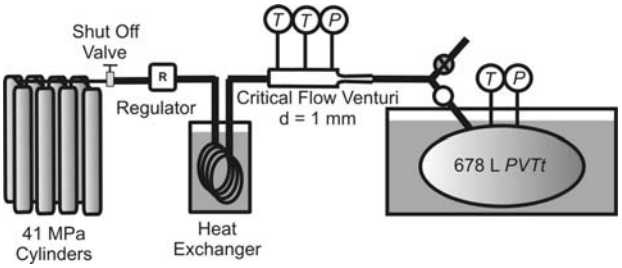

Fig. 7 Schematic of equipment used for calibration of the CFV under steady state conditions.

A plot of C_d versus the inverse square root of the theoretical Reynolds number for the 1 mm CFV is shown in Figure 8 along with a best fit curve used to calculate C_d for the CFV flow measurements. The theoretical Reynolds number is calculated using the theoretical mass flow, *i.e.* using C_d = 1 in Equation 3. At Re_{th} of approximately 4×10^5 ($Re_{th}^{-1/2}$ = 0.0016), the C_d curve departs from linearity due to the laminar to turbulent transition of the boundary layer [7]. A rational function (a quotient of 2 second order polynomials) was used to predict C_d for a given Re_{th} during the blow-down tests.

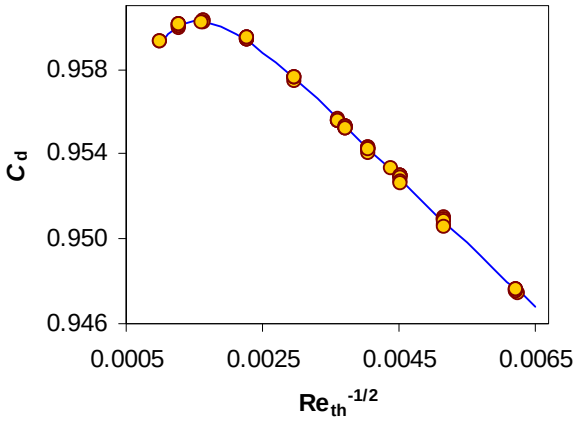

Fig. 8 Discharge coefficient versus the inverse square root of Reynolds number. Laminar to turbulent transition occurs at the lower $Re_{th}^{-1/2}$ values.

* k = 2, i.e. approximately 95 % confidence level value.

5. COMPARISONS OF INTEGRATED CFV MASS $\int \dot{m}\,dt$ AND COLLECTED MASS $\Delta\rho V$

5.1 Steady State Temperature and Pressure

The data reduction software that compares $\int \dot{m}\,dt$ and $\Delta\rho V$ was tested under steady state temperature, pressure, and flow conditions before using it to analyze transient flows. A pressure regulator and heat exchanger were placed between the gas source and the CFV as shown in Figure 9.

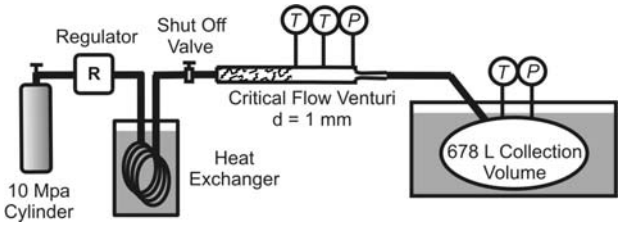

Fig. 9 Test arrangement for steady state flow tests.

In this test, the integrated mass flow from the CFV agreed with the mass collected in the *PVTt* tank within 0.01 %. This is expected because the same collection volume was used to measure the steady state C_d values and to measure $\Delta\rho V$; however, this test is essential to validate the algorithms used for CFV flow calculations and their integration.

5.2 Steady State Temperature, Transient Pressure

In the next set of experiments, $\int \dot{m}\,dt$ and $\Delta\rho V$ were compared using the equipment shown in Figure 10, *i.e*. with a heat exchanger between the blow-down tank and the CFV approach tube.

Except for 2 s long spikes caused by opening and closing the shut-off valve, the heat exchanger maintained the CFV gas temperature at 294.5 K ± 1 K during the filling process. Four steady-state-temperature / transient-pressure tests were performed. The differences between $\int \dot{m}\,dt$ and $\Delta\rho V$ for the four tests averaged +0.04 % with standard deviation of 0.04 %. These results are within our expected uncertainty of 0.14 % (k = 2) for this test (see Uncertainty Appendix).

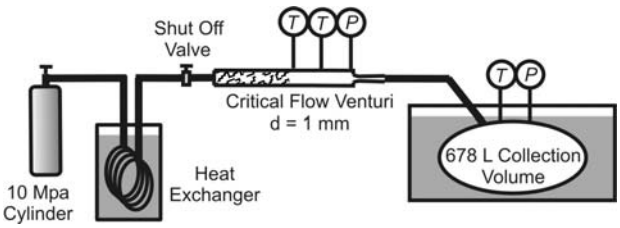

Fig. 10 Test arrangement for steady state temperature, transient pressure tests.

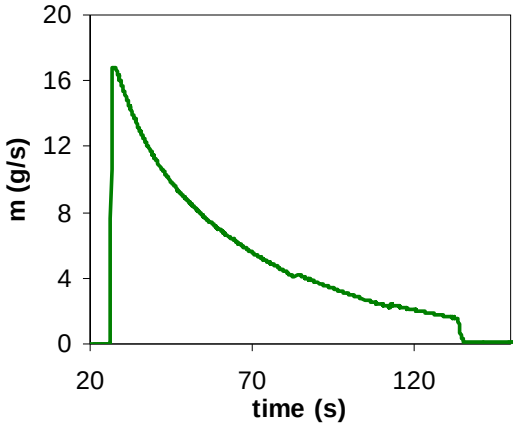

Fig. 11 Mass flow calculated from the CFV during a transient *T* and *P* blow-down test.

5.3 Transient Temperature and Pressure

In the next set of transient experiments, both the heat exchanger and the regulator were removed as depicted in Fig. 3. Hence, both temperature and pressure dropped dramatically as the blow-down tank emptied. Figure 11 shows the mass flow measured by the CFV for one of these tests in which the difference between $\int \dot{m}\,dt$ and $\Delta\rho V$ was –0.39 %.

The pressures and temperatures measured with the fast sensors are plotted in Figures 12 and 13. Opening the shut-off valve causes a rapid increase in pressure and an upward temperature spike due to heat of compression. A similar downward temperature spike occurs when the shut-off valve is closed. The thermocouple measurements used to calculate T_0 are also plotted in Figures 12 and 13.

Our results are remarkably sensitive to the measurement of the temperature T_1 of the gas at the CFV's throat. For example, if one assumed $T_1 = tc_1$ instead of using Eq. (4), the difference

between $\int \dot{m}\, dt$ and $\Delta\rho V$ would be +0.31 % instead of -0.39 %.

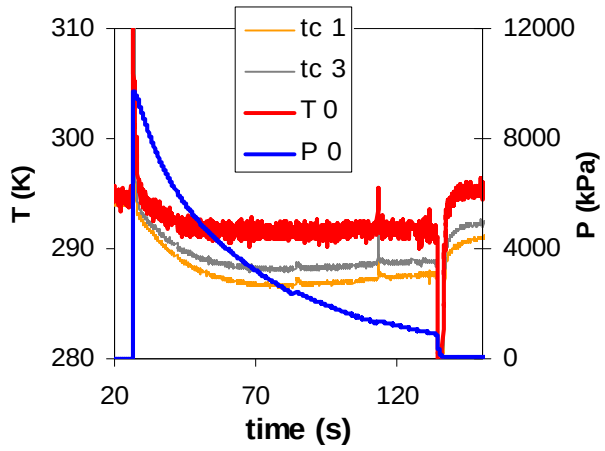

Fig. 12 CFV pressure and temperature during a transient T and P blow-down test. T_0 is the stagnation temperature at the CFV inlet (calculated from T_1).

The transient temperature and pressure test was repeated four times and the average difference between $\int \dot{m}\, dt$ and $\Delta\rho V$ was (–0.38 ± 0.01) %. (0.01 % is one standard deviation.). The differences exceed our predicted uncertainty of 0.29 % (k = 2, see Uncertainty Appendix) and lead one to the question, which uncertainty components are underestimated in the analysis? The relatively long 100 s time scale of the tests leads to the conclusion that the differences are not due to the pressure and temperature sensor time constants. Because the differences are much larger than the differences for the steady-state-temperature / transient-pressure tests, temperature measurement problems are probably the source of the error. We explore the two most likely sources in the following sections.

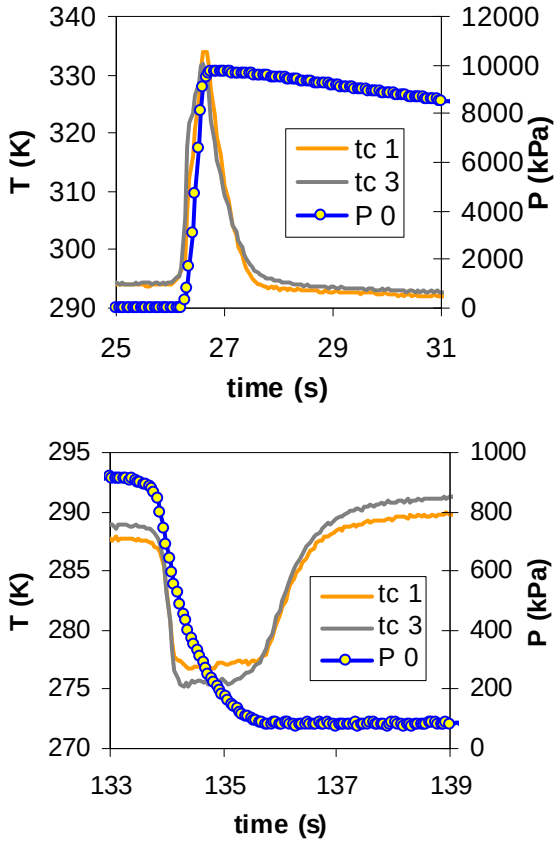

Fig. 13 Zoomed views of the test start and stop intervals showing pressure and thermocouple temperature measurements used to calculate T_0.

6. CFV TEMPERATURE MEASUREMENT ERRORS

Perhaps the most surprising outcome of the present research is the degree that widely used temperature measurement methods can contribute to the uncertainty of CFV flow measurements. Large temperature gradients often occur in the piping and gas near a CFV and this leads to significant errors in the stagnation temperature, T_0.

The arrangement shown in Figure 14 was used to demonstrate the problem. The 678 L *PVTt* standard was used to measure C_d values for the 1 mm CFV. A 3 mm sheathed thermistor was installed at the upstream temperature tap and a pair of fast thermocouples as described in Section 3 were installed at the downstream tap. Also, a thermistor was placed in contact with the CFV body, under a layer of insulation (as in Figure 4).

Temperature traces and C_d values are shown in Figure 15. In this test, the CFV pressure was regulated to be 3.2 MPa ± 0.1 MPa. Initially, cold gas due to the expansion of the gas from 41 MPa to 3.2 MPa at the regulator leads to a rapid drop in all temperatures. As the gas pressure in the source cylinders drops, the cooling capacity of the gas exiting the regulator decreases.

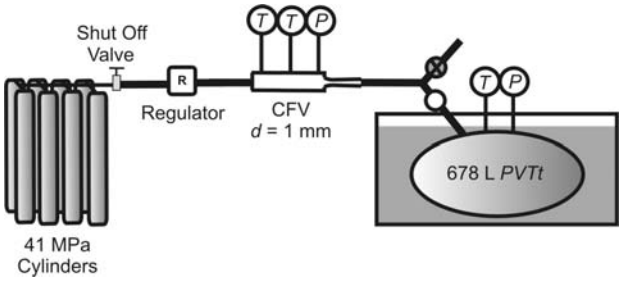

Fig. 14 Test set up used to investigate temperature measurement uncertainties in CFVs.

After about 30 minutes, all temperatures increase. The temperature measured by the thermocouple and thermistor take approximately 50 min to reach their minimum values. A second gas expansion occurs through the CFV; it cools the nozzle's body. The cold CFV body cools the upstream piping by conduction which, in turn, cools the gas at the temperature sensors. The thermistor and thermocouple are both mounted on the approach tube centerline, separated by 7 cm, but they differ by as much as 7 K, due to differences in their time constants and stem conduction errors in the thermistor. In summary, there are large, time-dependent, axial and radial temperature gradients in the approach tube. To illustrate the errors this introduces, the C_d values resulting from using the thermistor and thermocouple readings are plotted in Figure 15 and they differ by as much as 0.6 %. This example demonstrates that it can be challenging to obtain an accurate measurement of the temperature of the gas immediately upstream from the CFV. In this work, we extrapolated the readings of two thermocouples displaced in the streamwise direction, but more sophisticated approaches are needed because temperature measurement errors are a major uncertainty contributor to CFV flow measurements.

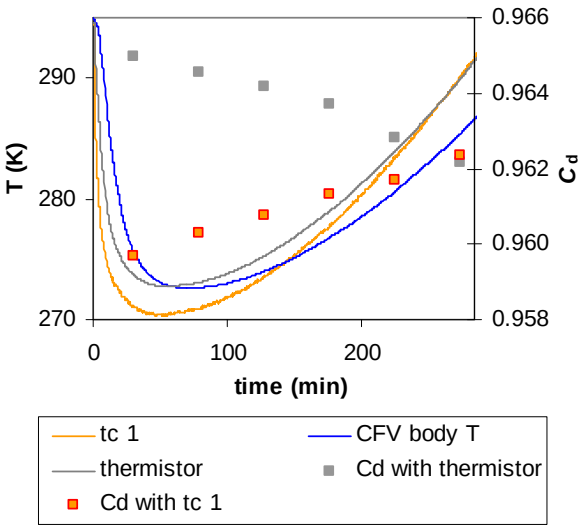

Fig. 15 Temperature traces and C_d values for a *PVTt* CFV calibration without a heat exchanger, illustrating C_d differences due to different temperature measurement methods.

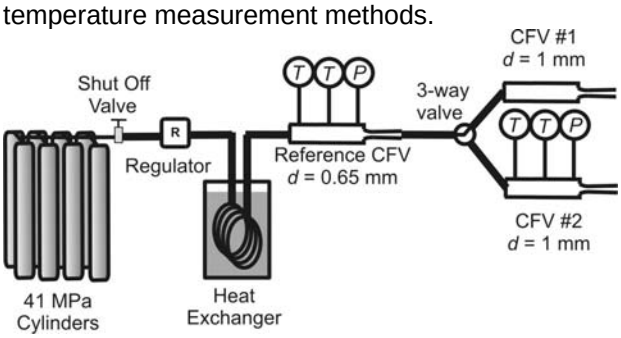

Fig. 16 CFVs arranged in series to measure thermal effects on $C_d A$.

7. THERMAL EFFECTS ON $C_d A$

Prior researchers [8] have measured the effects of temperature on the discharge of CFVs. There are two thermal effects: 1) thermal expansion of the CFV material changes its throat diameter and, 2) the CFV wall temperature affects the mass flux of gas in the thermal boundary layer [9, 10]. Predicting and correcting the changes in the product $C_d A$ from thermal effects is challenging for several reasons. The temperature of the CFV body depends on the cooling via the isentropic expansion of the flow, the heat transfer to the CFV from its surroundings, and heat conduction to the CFV via the inlet and outlet piping. All of these phenomena depend on the details of the specific CFV and its installation and many are time dependent.

We used the experimental set up shown in Figure 16 to study the magnitude of thermal effects on $C_d A$ for the CFV used in the transient tests. Steady state flow was established through a calibrated 0.65 mm CFV and CFV #1 with a regulator and heat exchanger upstream. During this equilibration period, CFV #2 remained at zero flow and at room temperature conditions. Once flow readings from the 0.65 mm reference CFV reached steady state (> 15 min), the 3-way valve was used to switch flow to CFV #2. CFV #2 was instrumented with the same fast pressure and temperature sensors described in Section 3. The CFVs and their approach tubes were insulated and 3 mm sheathed thermistors were used to measure the external temperature of CFV #2. The mass flow from the reference CFV was used to calculate the C_d for CFV #2 and it is plotted versus time in Figure 17, along with T_0 and the body temperature for CFV #2.

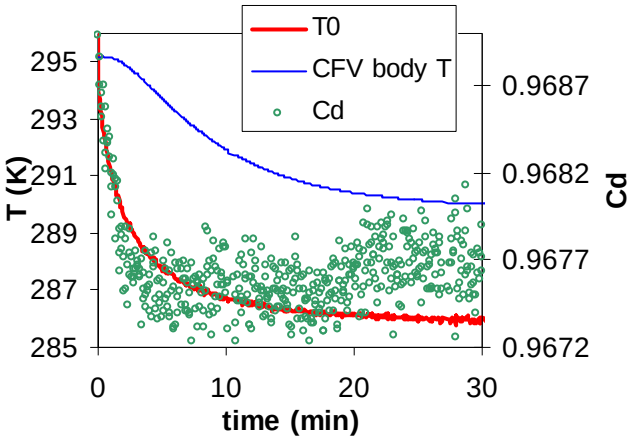

Fig. 17 Temperatures and C_d values observed upon sudden flow initiation in a 1 mm CFV.

The $C_d A$ values in Figure 17 drop 0.15 % over a 4 min interval.

Other iterations of this test have been conducted at other pressures, with and without the heat exchanger installed, and we have found that there is a nearly linear relationship between the final CFV body temperature and the change in $C_d A$ with $(dC_d A / dT_{CFV}) / C_d A = 2.7 \times 10^{-4}$. This value is in excellent agreement with the results given in Fig. 8 of Bignell and Choi [8] who obtained $(dC_d A / dT_{CFV}) / C_d A = 2.8 \times 10^{-4}$ for a heated 1 mm diameter CFV with very different design and temperature instrumentation.

8. CONCLUSIONS

Blow-down tests confirm that critical flow venturis accurately measure flow under transient conditions. Under transient pressure and steady state temperature conditions, we obtained agreement of 0.04 % between numerically integrated CFV flows and the mass accumulated in a collection volume. Under transient pressure and temperature conditions, the agreement was -0.38 %. The difficulty in measuring the gas temperature entering the CFV seems the most likely cause of the disagreement under transient temperature conditions, followed by thermal effects on the discharge coefficient due to thermal expansion of the throat and thermal boundary layers.

Further research is needed on thermal effects on the product $C_d A$ with the goal being a correction to the CFV flow based on the CFV body temperature and the gas temperature.

Large temperature gradients and temporal temperature changes occur in many CFV applications due to gas cooling as it expands through pressure regulators and the CFV, conduction along the material walls, and heat transfer to the surroundings. Temperature sensors suffer from stem conduction errors and slow time response. These errors in temperature measurement cause significant flow measurement errors. Better temperature measurement approaches are needed than those given in the current ISO [2] and ASME standards for CFVs. In this work we used two fast thermocouples separated along the pipe axis to extrapolate the gas temperature at the CFV entrance.

Now that the CFV has been demonstrated to measure flow accurately over the relatively long time scales in this work (100 s), they should be evaluated in more demanding transients, such as pulsatile flow.

APPENDIX: UNCERTAINTY ANALYSIS OF THE DIFFERENCE: $\int \dot{m}\, dt - \Delta\rho V$

Table 1 lists four categories of the uncertainty sources for the difference between $\int \dot{m}\, dt$ and $\Delta\rho V$ for the transient experiments. Normalized sensitivity

coefficients are unity for most components but are ½ for the quantities under the square root in the CFV mass flow equation. Some explanations of the uncertainty components follow.

Components 2, 3, 5, and 6: Uncertainties related to measurement of CFV pressure and temperature are listed twice, once for the C_d determinations using the *PVTt* standard and a second time for the usage of the CFV to measure mass flow. This was done because slow pressure sensors were used for the steady state C_d determinations and fast pressure sensors were used for the transient tests. In the case of temperature, sampling uncertainties related to spatial non-uniformity are considered dominant and these are not correlated between calibration and usage of the CFV. Pressure uncertainties are based on comparisons of redundant sensors (when available) and calibration histories. Temperature uncertainties are based on comparison of redundant sensors, calibration records, and estimates of spatial non-uniformity. For the test with a heat exchanger upstream, the temperature uncertainty used was 0.11 K (k = 1). For tests without a heat exchanger, 0.5 K (k = 1) was assumed.

Component 4: This component accounts for offsets in the C_d observed between periodic calibrations. We suspect that the changes resulted from opening and closing the high pressure taper seal fitting. Different torques applied in closing the fitting lead to different stress on the CFV body that change the CFV throat diameter.

Component 7: Prior researchers [8] have measured changes in C_d as a function of time, presumably due to the CFV gradually reaching thermal equilibrium with the gas. Further experiments were conducted on this question (see Section 7) and they are the basis for the value used in Table 1.

Component 8: Because the total integration time is > 100 s and the P and T sensor time constants are < 100 ms, the response time is not a significant uncertainty component for this experiment.

Components 9 and 10: Uncertainties in C^* are correlated between CFV calibration and usage. Care was taken to maintain the nitrogen purity, so molecular mass molecular mass uncertainty is not significant.

Component 11: Time labels in data files are based on a computer clock. The clock was checked against the NIST time reference and found correct to 7 parts in 10^6.

Components 12 and 13: Numerical errors caused by using the trapezoidal rule were estimated. Also, there are intervals at the start and stop of up to 300 ms during which the pressure is less than 150 kPa and the CFV is not under critical flow conditions. These intervals were not included in the numerical integration; however during these intervals gas moved through the nozzle into the collection volume. Equation 3 will over-report the mass flow during these non-critical conditions. By including the non-critical intervals in the numerical integration, we obtained an estimate of the uncertainty from the “non-critical tails”.

When the root-sum-square of all components is calculated, a k = 2 uncertainty of 0.29 % results. The largest uncertainty contributors are: 1) CFV temperature and pressure measurements during the transient test and 2) thermal effects on C_d. When the uncertainty analysis shown in Table 1 is modified for the transient pressure and steady state temperature test, the thermal equilibrium and temperature measurements are reduced and the expanded uncertainty is 0.14 %.

Table 1. Uncertainty for the difference $\int \dot{m}\, dt - \Delta\rho V$ for the transient *T* and *P* test.

Uncertainty Component	Normalized Sensitivity (-)	Uncertainty (k = 1, %)
A) C_d from *PVTt* cal		
1. *PVTt* standard	1	0.0125
2. *P*	1	0.02
3. *T*	0.5	0.010
B) CFV mass flow		
4. C_d stability	1	0.025
5. *P*	1	0.05
6. *T*	0.5	0.169
7. Thermal effects on C_d	1	0.1
8. *P* and *T* resp time	1	0.01
9. *C**	1	< 0.001
10. *R, M*	0.5	< 0.001
C) Integration		
11. Time	1	< 0.001
12. Numerical errors	1	0.005
13. Non-critical tails	1	0.005
D) $\Delta\rho$ *V*		
14. $\Delta\rho$	1	0.007
15. *V*	1	0.01
Combined Unc. (k = 1)		0.15
Expanded Unc. (k = 2)		**0.29**

REFERENCES

[1] Cascetta, F., Rotondo, G., and Musto, M., *Measuring of Compressed Natural Gas in Automotive Application: A Comparative Analysis of Mass Versus Volumetric Metering Methods*, Flow Meas. Instrum., **19**, pp. 338 – 341, 2008.

[2] ISO 9300, *Measurement of Gas Flow by Means of Critical Flow Venturi Nozzles*, Geneva Switzerland, 2005.

[3] Wright, J. D., Johnson, A. N., Moldover, M. R., and Kline, G. M*., Gas Flowmeter Calibrations with the 34 L and 677 L PVTt Standards*, NIST Special Publication 250-63, National Institute of Standards and Technology, Gaithersburg, Maryland, (2004).

[4] Lemmon, E. W., McLinden, M. O., and Huber, M. L., Refprop 23: Reference Fluid Thermodynamic and Transport Properties, NIST Standard Reference Database 23, Version 8.0, National Institute of Standards and Technology, Boulder, Colorado, April, 2007, www.nist.gov/srd/nist23.htm.

[5] Wright, J. D. and Johnson, A. N., *Uncertainty in Primary Gas Flow Standards Due to Flow Work Phenomena*, FLOMEKO, Salvador, Brazil 2000.

[6] Wright, J. D. and Johnson, A. N., *Lower Uncertainty (0.015 % to 0.025 %) of NIST's Standards for Gas Flow from 0.01 to 2000 Standard Liters / Minute*, Proc. of the 2009 Measurement Science Conference, Anaheim, CA, 2009.

[7] Johnson, A. N. and Wright, J. D., *Comparison between Theoretical CFV Flow Models and NIST's Primary Flow Data in the Laminar, Transition, and Turbulent Flow Regimes*, ASME J. of Fluids Eng., **130**, pp. 1-11, 2008.

[8] Bignell, N. and Choi, Y. M., *Thermal Effects in Small Sonic Nozzles*, Flow Meas. Instrum., **13**, pp. 17 – 22, 2002.

[9] Johnson, A. N., *Numerical Characterization of the Discharge Coefficient in Critical Nozzles*, Ph.D. Thesis, Pennsylvania State Univ., University Park, Pennsylvania, USA, 2000.

[10] Wright, J. D., *Uncertainty of the Critical Venturi Transfer Standard Used in the K6 Gas Flow Key Comparison*, Proceedings of FLOMEKO, Johannesburg, South Africa, 2007.